

Diverse Inactivation Mechanisms of the PenA1 Carbapenemase from *Burkholderia multivorans*

Michiyoshi Nukaga¹ and Tyuji Hoshino^{2,*}

¹ Faculty of Pharmaceutical Sciences, Josai International University,
Gumyo 1, Togane-shi Chiba 283-8555, Japan

² Graduate School of Pharmaceutical Sciences, Chiba University,
1-8-1 Inohana, Chuo-ku, Chiba 260-8675, Japan

1 Introduction

Burkholderia cepacia complex (Bcc) is a group of Gram negative bacteria that are opportunistic pathogens and pose a serious threat to those with cystic fibrosis or compromised immune systems. All Bcc carry an inducible chromosomal class A serine β -lactamase of the PenA-family; the spectra of hydrolytic activity for each PenA family member varies by species as well as within species due to sequence heterogeneity.

One strategy to combat β -lactamase-mediated antibiotic resistance is to combine a β -lactam with a β -lactamase inhibitor. β -Lactamase inhibitors possess the potential to be of great importance for treating infections as they rescue β -lactams from hydrolysis by β -lactamases. There are three major classes of β -lactamase inhibitors that are active against class A serine enzymes: β -lactam-based (e.g., clavulanic acid, tazobactam, enmetazobactam), diazabicyclooctanes (DBOs) (e.g., avibactam and relebactam), and boronates (e.g., vaborbactam). The inhibitors' mechanisms of action with β -lactamases vary by type.

β -Lactam-based inhibitors form acyl-complexes with the β -lactamase active site but are rapidly converted to various intermediates (imine, cis- and trans-enamine), can fragment, and are eventually hydrolyzed to inactive products. The β -lactam-based inhibitors, clavulanic acid, sulbactam, and tazobactam, were the first to reach clinical use. Interest in this class has continued as a novel sulfone, enmetazobactam (formerly AAI101), partnered with cefepime is currently being evaluated in clinical trials. Enmetazobactam is a zwitterion, which results in enhanced bacteria cell penetration as well as potent β -lactamase inactivation rates.

DBOs also form an acyl-complex with the active site; however, this process is reversible and active inhibitor can be released upon recyclization of the DBO scaffold. As with β -lactam-based inhibitors, DBOs are also hydrolyzed, albeit the rate is slow, and with serine β -lactamases, typically after desulfation of the inhibitor. Two DBOs, avibactam and relebactam, are approved by the U.S. Food and Drug Administration (FDA) paired with ceftazidime and imipenemcilastatin, respectively. Ceftazidime-avibactam is the first β -lactam- β -lactamase inhibitor combination approved to treat Enterobacterales-producing KPC-type carbapenemases, thus targeting a CDC urgent

health threat. Several novel "dualaction" DBO β -lactamase inhibitors (e.g., durlobactam, zidebactam, and nacubactam) that also inactivate penicillin binding proteins are in development.

Boronate inhibitors form a dative bond between the boron atom of the inhibitor and the active site serine hydroxyl, which is reversible and results in the release of an active inhibitor. To date, hydrolysis of boronate inhibitors by β -lactamases is not described, likely due to the unique chemistry of these compounds that precludes hydrolysis. One boronate, vaborbactam, is approved for use with meropenem by the FDA in the United States. Novel boronates (e.g., taniborbactam and QPX7728) that possess the most extensive β -lactamase inhibition profiles (classes A, B, C, and D) are in the pipeline.

Inhibiting the PenA β -lactamase with β -lactams that are poor substrates for the β -lactamase and/or the addition of a β -lactamase inhibitor is an essential criterion for antimicrobial activity against Bcc. Previously, avibactam was found to be a potent inactivator of the PenA1 β -lactamase from *Burkholderia multivorans*, a member of Bcc. Here, the activity of three newer β -lactamase inhibitors from all three classes, enmetazobactam, relebactam, and vaborbactam, are tested against PenA1 and compared to avibactam, clavulanic acid, and tazobactam. Moreover, the contribution of selected amino acids in various active site motifs (S70XXK73, S130DN132, R164- Ω -loop-D179, K234TG) toward inhibition is evaluated by making single amino acid substitutions (S70A, K73A, S130A, E166A, N170A, R220A, K234A, T237A, and D276A) in PenA1. The roles of these motifs in PenA1 is that S70 is the nucleophile, K73, S130, E166, and K234 participate in acylation and deacylation, K234, R220, and D276 are involved in binding and stabilization, and E166 and N170 anchor the deacylation water molecule.

2 Experiment

Crystallography.

The expression plasmid was constructed with codons optimized for expression in *E. coli* and cloned into pET48b(+) expression vector with an human rhinovirus (HRV) 3C cleavage site before its multiple-cloning site. The N-terminal Ala-Arg of PenA was replaced by Gly-Pro-Leu-Gly-Ser (3 amino acids addition) to allow for cleavage by the HRV 3C protease. The R220A substitution

was constructed by conducted site-directed mutagenesis of the nucleotides corresponding to position 220 using the Quikchange XL mutagenesis kit as described above. The R220A variant was purified by a HisTrap FF crude column (GE Healthcare) equilibrated with 20 mM sodium phosphate buffer pH 7.4, 20 mM imidazole, 0.5 M NaCl, followed by the cleavage of His-tag by HRV 3C protease. The cleaved protein was again purified by using the HisTrap HP column (GE Healthcare). HiTrap SP HP (GE Healthcare) equilibrated with 20mMMES buffer, pH 6.3 was used for the next step and eluted with a 0–0.5 M NaCl gradient. The protein was further purified by gel filtration using a HiLoad 16/60 Superdex 200 pg (GE Healthcare) system with a running buffer of 20 mM HEPES pH 7.5 and 100mMNaCl. The protein was concentrated to 15 mg/mL.

The R220A variant β -lactamase was crystallized at room temperature by the vapor diffusion method using a 250 μ L reservoir (25% polyethylene glycol 8 kDa [PEG8K], 0.1MMES at pH 6.5)) with a 4 μ L hanging drop (7.5 mg/mL protein, 12.5% PEG8K, 0.05 M MES at pH 6.5). Adding acetone to the drop (final 4%) improved the crystal size and shape. The R220A variant crystal was cryoprotected by the addition of 20% glycerol to the PEG holding solution. Loop-mounted crystals were flash-cooled and kept at 100 K with a nitrogen gas stream. The 1.0° oscillation images were collected on a Pilatus3 S2M detector at NW12A beamline. The XDS programs were used to reduce and scale Xray intensities (Table 1). Molecular replacement using the PenA1 structure (PDB 3W4Q) as a search model and model refinement were done using the PHENIX program. Coot was used for manual model fitting. The resolution limit was determined so that the I/σ would be higher than 2.0. PDB code is 7D5J.

MD Simulation and Analysis of Simulation Results.

The initial coordinates of the atoms in PenA1 and R220A β -lactamases were respective crystal structures. The crystal waters except for the deacylation and oxyanion waters were removed, and then water molecules were generated around the substrate and enzyme by the 3D-RISM atom placement algorithm. The β -lactamases were placed in a rectangular box filled with TIP3P water molecules. The model also contains sodium and chloride ions to neutralize the model system. The final model size was ca. 80 Å \times 70 Å \times 87 Å and the total number of atoms was about 48 000 for both models. The ff14SB force field was applied to the enzyme. Minimization, heating, and pre-equilibration were carried out using the sander module of AMBER18. Production run of MD simulation was carried out using the pmemd module. The production runs of MD simulation were carried out for 200 ns. The cutoff distance for the electrostatic and van der Waals energy terms was set to 12.0 Å. The particle mesh Ewald method was applied to calculate the long-distance electrostatic force. The integration time step was 1 fs. The ptraj module was utilized to obtain the snapshot structures from the simulation trajectory, the root-mean-square deviation (RMSD), and the B-factor. In the calculation of the B-factor, only main chain atoms (N, Ca, and C) were taken into account.

Table 1. X-ray Data Collection and Refinement.

parameter	value
X-ray data collection (XDS)	
detector	Pilatus3 S2M
wavelength (Å)	1.000
space group	C2
cell dimensions	
<i>a</i> , <i>b</i> , <i>c</i> (Å)	123.3, 71.2, 84.5
α , β , γ (deg)	90, 90.04, 90
resolution (highest.shell) (Å)	42.27–1.51 (1.53–1.51)
observations	44 234 990 (19 251)
unique reflections	114 986 (5243)
completeness (%)	98.2 (93.0)
redundancy	3.8 (3.7)
$I_{av}/\sigma(I)$	12.5 (2.5)
CC1/2	0.988 (0.640)
$R_{merge}(I)$	0.056 (0.365)
refinement results (Phenix)	
resolution range (Å)	34.88–1.51 (1.56–1.51)
no. of reflections used	113 426 (10 858)
R_{work}/R_{free} (%)	17.19 (23.77)/19.10 (27.37)
R_{total} (%)	17.27
Ramachandran zones (%)	
favored/allowed/disallowed	98.7/1.3/0
RMSD values from ideality	
bond lengths (Å)	0.005
bond angles (deg)	0.83
mean B-factors (number of atoms)	
protein (no.)	15.43 (5730)
MES (no.)	27.05 (36)
water molecules (no.)	24.00 (732)
all atoms (no.)	16.45 (6498)

3 Results and Discussion

To understand the mechanistic contribution of R220 toward β -lactamase inhibition, the R220A variant of PenA1 was crystallized (Table 1) [1]. The R220A crystal structure (PDB 7D5J) was obtained at 1.5 Å resolution at pH 6.5, while the previously published PenA1 crystal structure (PDB 3W4Q) was at a 1.2 Å resolution at pH 4.2. The R220A and PenA1 β -lactamase crystals were in the space group C2 with three molecules per asymmetric unit and in a monomeric state with protein B-factors of 15.43 Å² and 16.39 Å², respectively. The overall structures of PenA1 and the R220A variant were very similar (rms deviation is 0.29 Å for 35–285 Ca atoms) with protein folds consisting of an α -helical region followed by five antiparallel β -sheet strands and additional α -helices. Active site residues (S70, K73, S130, N132, E166, N170, K234, T235, G236, and T237) were well modeled in the 2F_o–F_c map (Figure 1a) and were superimposable (Figure 1b) with a RMSD of 0.39 Å for all the atoms present in these amino acids. A higher RMSD was mainly caused by a different rotamer of residue T237. The R220A substitution did not affect the overall active site

architecture as evidenced by 0.39 Å rms deviation for active site residues.

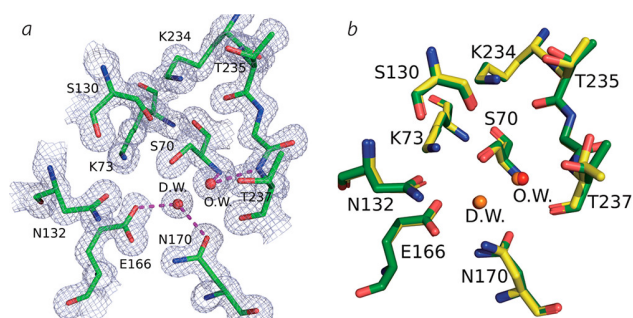


Figure 1: (a) 2Fo-Fc electron density map (1.5σ) around the active site of R220A variant enzyme. O.W., oxanyon water; D.W., deacylation water. (b) Superposition of PenA1 (yellow, PDB 3W4Q) and the R220A variant (green, PDB 7D5J).

In the wild-type PenA1 structure, the guanidium group of R220 formed a four membered intramolecule hydrogen bonding network, R220:NH1-D245:O (3.1 Å distance), R220:NH1-G236:O (2.9 Å), R220:NH2-T237:OG (3.0 Å), and NH2:NED276:OD1 (2.7 Å) (Figure 2a). In the R220A variant, four water molecules, W3, W4, W5, W6 of ChainA, now occupied the space normally occupied by the guanidium side chain of arginine and the major hydrogen bonds between 237 and 220–276 were lost (Figure 2b). As a result, the positioning of D276:OD1 was also moved by 2.7 Å and the side chain of D276 lacked electron density (Figure 2c). The B-factor of Ca in the A270-D276 region increased with the loss of the hydrogen bonds and migration of D276.

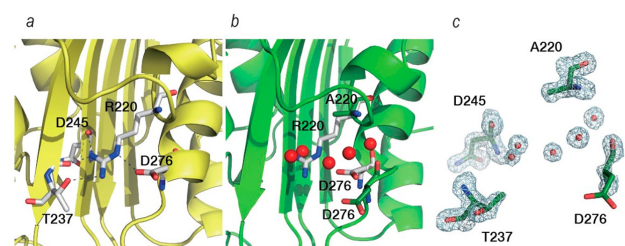


Figure 2: Residues around position R220 of PenA1 (PDB 3W4Q) (a) and A220 of the R220A variant (PDB 7D5J) (b). White sticks show R220 of PenA1 and its hydrogen-bonding network (dashed back lines). Green sticks show A220 and D276 of the R220A variant. Red spheres in (b) are water molecules observed near the A220 of the R220A variant. Electron density around A220 (PDB 7D5J) reveals the occupancy by water molecules due to loss of the guanidium and unresolved density for the carboxylate of D276 (c).

The B-factor of Ca in the A270-D276 region increased with the loss of the hydrogen bonds and migration of D276 (Figure 3). Whereas average B-factors for PenA1 and the R220A variant were 16.39/15.43 for the whole molecule, they were 20.87/25.01 for the Ca atoms of the A270-D276 region, and 17.62/24.26 for the A274-D276 region, respectively. Moreover, the B-factor of Ca in the V225-G228 region of the R220A variant was also increased as well as the area around P254. Although two different traces were modeled in this region in wild-type PenA1, the second trace could not be built in 2Fo-Fc map of the R220A variant. Overall, the three regions in α/β domain of the R220A variant possessed higher B-factors than PenA1.

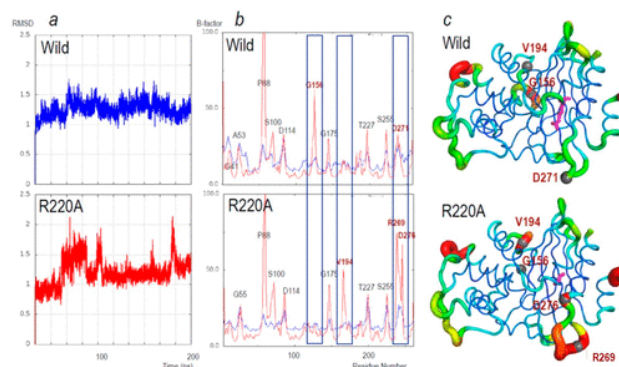


Figure 3: (a) Changes in the root-mean-square deviation (RMSD) for main-chain atoms during the 200 ns simulations relative to the starting structure. Upper, PenA1 (wild, blue lines) and lower, R220A (R220A, red lines). (b) Average B-factors of main-chain atoms of the individual amino acid residues during the 200 ns MD simulations (red); the average B-factors of the crystal structure (blue). Upper: PenA1 (Wild) and Lower: R220A (R220A). Labels on the peak indicate the residue using standard class A β-lactamase numbering. Residues with the largest changes in B-factor are in red font and highlighted by blue rectangles. (c) B-factors from MD simulation putty representation on Pymol of (upper) PenA1 and (lower) R220A. The color changes from blue (B-factors below 5.0), while cyan, green, yellow, and red (B factors of more than 50.0). The thickness of the lines reflects the height of the B-factor. The stick model (magenta) indicates the position of R220 and A220, respectively. Sphere atom models and red font indicate the peak position found in panel (b).

To further analyze the movement of the β-lactamases, molecular dynamics (MD) simulations were performed using the crystal structures of PenA1 (PDB 3W4Q) and the R220A variant (PDB 7D5J). RMSD value of the R220A variant for main chain atoms from the initial structure was relatively unstable compared to PenA1 (Figure 3a). This observation suggests that the movement of main chain amino acids of the R220A variant is larger than for PenA1. The average B-factors for main chain atoms calculated from MD simulation trajectories are shown in Figure 3b and 3c. The B-factor peaks were clearly different in three regions between PenA1 and the R220A variant. In the

R269-D276 region of the R220A variant, B-factors were clearly larger than PenA1. This may be the result of loss of the NH2:R220-OD1:D276 hydrogen bond. Other differences were observed in the region of G156 and V194. The former was disappearance of the peak at G156 and the appearance of a new peak at V194 for the R220A variant.

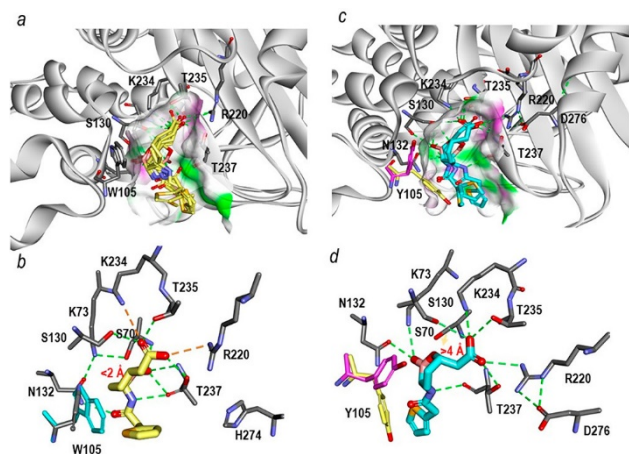


Figure 4: Michaelis–Menten complexes of vaborbactam in the sp₂ configuration shown in multiple different poses obtained upon docking into the active sites of KPC-2 (PDB 2OV5) and PenA1 (PDB 3W4Q). (a) Within KPC-2, several docked vaborbactam molecules (yellow) formed favorable complexes. The surface of the active site was colored by hydrogen-bonding type with hydrogen donors colored in magenta and hydrogen acceptors in green. The surface further reveals the difference in the active site sizes between the two enzymes with the KPC-2 active site being narrower than that of PenA1. (b) A close up of the active site interactions in KPC-2 with a single selected vaborbactam pose obtained from docking reveals favorable interactions with the boronate near S70 (<2 Å) and stacking interactions between W105 (cyan) and cyclic boronate moiety. Hydrogen bonds are represented by dashed green lines; stronger hydrogen bonding interactions (e.g., ionic interactions) are in orange dashed lines. (c) Conversely, with PenA1, the multiple poses of vaborbactam (cyan) obtained from the docking formed mostly unfavorable interactions that were driven by larger active site of PenA1. Surface representations are the same as described in panel (a) for KPC-2. (d) A close up of the PenA1 active site with a single selected vaborbactam pose obtained from docking reveals that the carboxylate moiety of vaborbactam competes for binding to K234 and T235, thus moving the boronate away from S70 (>4 Å); the faint orange arrow points out the distance between hydroxide side chain of S70 and the boronate moiety. Moreover, during docking two conformations of Y105 (pink/yellow) were observed that competed for interactions with cyclic boronate moiety and the thiophene ring of vaborbactam. The hydrogen bonding interactions are the same as described in panel (b) for KPC-2.

To gain insight into why vaborbactam is the worst inhibitor of PenA1 (k_2/K_m , $3.4 \pm 0.1 \times 10^2 \text{ M}^{-1} \text{ s}^{-1}$) in vitro, Michaelis–Menten complexes were generated with PenA1 and vaborbactam and compared to Michaelis–Menten complexes of KPC-2 and vaborbactam, as vaborbactam is a potent inactivator of KPC-2. The KPC-2 active site is narrower than that of PenA1; thus, during docking into KPC-2, vaborbactam was restrained into a conformation, which allowed for productive interactions (Figure 4a). In KPC-2, the boronic acid moiety was “guided” toward the S70 within $\approx 2 \text{ \AA}$, due in a major part to W105 maintaining steric interactions with the cyclic boronate region of vaborbactam to promote favorable complex formation. Conversely, the active site of PenA1 is larger allowing vaborbactam to form different conformations and interactions within the active site during docking. Besides the larger active site of PenA1, another factor that influenced vaborbactam binding was that PenA1 has a tyrosine at position 105 as opposed to a tryptophan in KPC-2 (Figure 4b). Position Y105 in PenA1 was very flexible, flipping more than 90° . The movement of Y105 further restricted the access of vaborbactam into the PenA1 active site by competing for binding between the cyclic boronate and thiophene rings on vaborbactam. With PenA1, the boronic acid moiety was prevented from making productive interactions with S70, due to multiple conformations that vaborbactam adopted. Furthermore, the molecular docking suggests that the interactions of the carboxylate group of vaborbactam with K234 and T235 was preventing the boronate from reaching S70 as it was more than 4.0 \AA away.

Acknowledgement

This study was partly supported by the Grant-in-Aid for Scientific Research (C) Grant Number 20K07484. This work has been performed under the approval of the Photon Factory Program Advisory Committee (Proposal No. 2020G590).

References

[1] M. Nukaga *et al.*, *ACS Infect. Dis.* **7**, 826 (2021).

* hoshino@chiba-u.jp